

ESTIMATING THE SIZE OF LATE VENEER IMPACTORS FROM IMPACT-INDUCED MIXING ON MERCURY

E. G. RIVERA-VALENTIN^{1,2} AND A. C. BARR^{1,2}

¹ Department of Geological Sciences, Brown University, 324 Brook Street, Box 1846, Providence, RI 02912, USA; rivera-valentin@brown.edu

² Center for Lunar Origin and Evolution, Southwest Research Institute, Boulder, CO 80302, USA

Received 2013 November 21; accepted 2014 January 12; published 2014 January 23

ABSTRACT

Late accretion of a “veneer” of compositionally diverse planetesimals may introduce chemical heterogeneity in the mantles of the terrestrial planets. The size of the late veneer objects is an important control on the angular momenta, eccentricities, and inclinations of the terrestrial planets, but current estimates range from meter-scale bodies to objects with diameters of thousands of kilometers. We use a three-dimensional global Monte Carlo model of impact cratering, excavation, and ejecta blanket formation to show that evidence of mantle heterogeneity can be preserved within ejecta blankets of mantle-exhuming impacts on terrestrial planets. Compositionally distinct provinces implanted at the time of the late veneer are most likely to be preserved in bodies whose subsequent geodynamical evolution is limited. Mercury may have avoided intensive mixing by solid-state convection during much of its history. Its subsequent bombardment may have then excavated evidence of primordial mantle heterogeneity introduced by the late veneer. Simple geometric arguments can predict the amount of mantle material in the ejecta blanket of mantle-exhuming impacts, and deviations in composition relative to geometric predictions can constrain the length-scale of chemical heterogeneities in the subsurface. A marked change in the relationship between mantle and ejecta composition occurs when chemically distinct provinces are ~ 250 km in diameter; thus, evidence of bombardment by thousand-kilometer-sized objects should be readily apparent from the variation in compositions of ejecta blankets in Mercury’s ancient cratered terrains.

Key words: accretion, accretion disks – planets and satellites: composition – planets and satellites: individual (Mercury)

Online-only material: color figures

1. INTRODUCTION

The abundance of highly siderophile elements (HSEs) in the mantles of the Earth, Moon, and Mars argues for the accretion of the final $\sim 1\%$ of their masses as a “late veneer” of leftover planetesimals arriving after the end of the giant impact phase, ~ 30 – 100 Myr after CAI formation, but before the asteroidal late heavy bombardment (LHB) at ~ 700 Myr (Tera et al. 1974; Hartmann et al. 2000; Drake & Righter 2002; Chambers 2004; Walker et al. 2004; Day et al. 2007; Kleine et al. 2009; Walker 2009). Dynamical scattering of late veneer bodies can modify the inclinations and eccentricities of the terrestrial planets along with modifying their spin angular momenta and obliquities via impacts (e.g., Chambers & Wetherill 1998; Bottke et al. 2010; Schlichting et al. 2012; Raymond et al. 2013); however, impactor size is not well-constrained. Schlichting et al. (2012) suggest that a leftover planetesimal population with radii $\lesssim 10$ m can account for the abundance of HSEs on the Earth, Mars, and the Moon, and provide sufficient dampening of the high eccentricities and inclinations expected after the giant impact phase in terrestrial planet accretion. Bottke et al. (2010) favor a size distribution dominated by extremely large bodies (~ 2500 – 3000 km) and stochastic accretion, which provides an explanation for why the abundance of HSEs on Earth relative to the Moon is significantly higher than what would be predicted by the relative impact probability onto each body. Raymond et al. (2013) suggest the large Earth/Moon HSE abundance ratio and planetary angular momenta can be reproduced if impact-induced erosion is considered, and large late veneer projectiles had diameters $\gtrsim 500$ – 1000 km, and possibly less than 2000 km.

Variations in the composition of planetesimals are expected due to radial chemical gradients in the solar nebula (e.g., Lewis

1972). The planetesimal population is expected to undergo significant radial mixing before the time of late veneer delivery due to scattering by planetary embryos (Chambers 2004). Accretion from this heterogeneous population may explain aspects of terrestrial geochemistry; for example, the increase in oxidation state inferred from mantle chemistry, which may be due to the delivery of FeO-rich (rather than Fe-rich) material (O’Neil 1991; Wood et al. 2006). Thus, late veneer impactors would also introduce variations into the concentrations of major rock-forming elements in the planets’ mantles.

Compositional heterogeneity may be preserved in the mantles of solid bodies that have not experienced a global magma ocean or vigorous mantle convection after late veneer deposition. The planet Mercury may be such a body. Mercury’s core occupies $\gtrsim 50\%$ (Hauck et al. 2013) of its interior, and its mantle is only ~ 400 km thick (Smith et al. 2012), which is only about $\sim 15\%$ – 20% of its radius (for comparison Earth’s mantle occupies $\sim 45\%$ of its radius). Solid-state convection in Mercury’s mantle, which would be expected to drive lateral mixing of the planet’s chemistry, could have been transient (Michel et al. 2013), and when it occurred, it would have been extremely sluggish and confined to a thin layer at the base of the mantle owing to the small Rayleigh number and stress-dependent viscosity (Redmond & King 2007). Mercury’s high mean density suggests to some that it suffered a planetary-scale impact during the final phases of its accretion, leading to significant loss of silicate (e.g., Benz et al. 2007). The remaining planet would be melted after this event, leading to vigorous mixing in its post-impact magma ocean; however, this may have happened before, or concurrently with, the late veneer (Raymond et al. 2013). Heterogeneities implanted into Mercury after it solidified may persist to the present.

Here, we develop a fully three-dimensional (3D) global Monte Carlo model of impact-induced mixing to show how the compositions of ejecta blankets formed from asteroidal impacts during the LHB can be used to infer the length-scale of subsurface heterogeneities. We show that model mercuries experiencing identical bombardment histories, but with different distributions of major elements in their mantles, will display statistically different ranges of ejecta blanket compositions. For a chemically homogeneous mantle, simple geometric arguments predict the abundance of mantle material in surface ejecta; deviations from the geometric predictions provide information about the length-scale of chemical heterogeneities in the subsurface. For crustal thicknesses <60 km, as is expected on Mercury, we find a marked change in the relationship between mantle and ejecta composition when the diameter of compositional provinces is comparable to the diameter of the transient crater created by the most common crust-penetrating impactor. Thus, bombardment by large late veneer impactors may be inferred from the composition of ejecta blankets.

2. METHODS

2.1. Bombardment

The number and clustering of lunar impact basins and ages of lunar rocks suggest the frequency of impacts onto the terrestrial planets increased ~ 700 million years after the endpoint of planet formation, during the so-called LHB (Tera et al. 1974; Hartmann et al. 2000). Simulations of the dynamical sculpting of the solar system suggest the LHB was triggered by the orbital migration of the outer planets (Tsiganis et al. 2005; Gomes et al. 2005), which caused a shower of asteroidal material to hit the terrestrial planets. The inner solar system bombardment is thought to have occurred in two stages (Bottke et al. 2012; Morbidelli et al. 2012). Before giant planet migration, asteroids occupying an extended zone of objects interior to the present-day asteroid belt, termed the E-belt, are scattered inward by Mars. In the second phase, giant planet migration causes the ν_6 secular resonance to sweep through the primordial asteroid belt, sending objects into the inner solar system with excited velocities depleting the E-belt, whose leftovers reside in the Hungaria population of asteroids (Bottke et al. 2012).

We use Monte Carlo methods to select a population of impactors with a total mass and size-frequency distribution (SFD) consistent with the inner solar system bombardment. The SFD of objects striking Mercury is assumed to be the same as that of the primordial asteroid belt, which is similar to the present-day belt (Bottke et al. 2005). Due to the resolution of our global model, we consider impactors with $D \geq 5$ km; thus, our SFD contains one slope break at $D = 100$ km and follows a differential power law in mass (m) of the form $dN/dm \propto m^{-1.7}$ for $D \leq 100$ km and $dN/dm \propto m^{-2.2}$ for $D \geq 100$ km (Bottke et al. 2005; Ivanov et al. 2002), assuming an impactor density of $\rho_i = 2700$ kg m^{-3} (Bottke et al. 2012; Britt et al. 2002). The total bombardment mass is constrained using the estimated total lunar bombardment mass, $\sim 3.5 \times 10^{19}$ kg (Day et al. 2007, 2010; Walker et al. 2004; Morbidelli et al. 2012), and assuming the total impacting mass on Mercury is ~ 1.82 times that on the Moon (Le Feuvre & Wieczorek 2011); a total of $\sim 6.4 \times 10^{19}$ kg of asteroidal material impacts Mercury. Mean impact velocities for Mercury are estimated to be a factor of 2.16 higher than on the Moon (Le Feuvre & Wieczorek 2011). We select velocities to follow a Rayleigh distribution around a mean of 26 km s^{-1}

and 45 km s^{-1} for the first and second bombardment stages respectively.

2.2. Three-dimensional Model

Mercury is represented by a Cartesian sphere of radius 2440 km and a core of radius 2000 km (Hauck et al. 2013) discretized into cubic volume elements 10 km on a side, giving $\sim 6.1 \times 10^7$ elements (cf., Barr & Canup 2010). Impact location is randomly chosen for longitude and latitude (φ) follows $d\varphi = \sin(2\varphi)$ (Barr & Canup 2010). An impactor of diameter D creates a transient crater of diameter D_{tc} , given by the Pi scaling law (Ivanov & Artemieva 2002),

$$D_{tc} = 1.16 \left(\frac{\rho_i}{\rho_m} \right)^{\frac{1}{3}} D^{0.78} (v_i \sin \Omega)^{0.43} g^{-0.22}, \quad (1)$$

where $\rho_m = 3700$ kg m^{-3} is Mercury's silicate density (Smith et al. 2012), v_i is impactor velocity, $g = 3.7$ m s^{-2} is Mercury's gravity, and Ω is impact angle. We use the Maxwell Z-model to determine the amount and provenance of material excavated during each impact. An impactor excavates a volume approximated by an oblate spheroid of diameter D_{tc} and depth $D_{tc}/8$; the total volume excavated is $V_{exc} = (\pi/48)D_{tc}^3$ (Maxwell 1977; Melosh 1989). Excavated material is assumed to be compositionally homogenized and redeposited on the surface within an annular ejecta blanket extending from the crater rim to $D_{tc}/2$ (Housen & Holsapple 2011; Osinski et al. 2011). Although some radial and vertical mixing of excavated material is expected during the excavation stage (Melosh 1989; Osinski et al. 2011), impact ejecta is not completely homogenized before deposition. This can be taken into account by averaging the composition of each continuous ejecta blanket before comparing our model results to observations.

Compositional heterogeneity in the mantle is modeled as spheres of diameter D_{prv} . For every Monte Carlo run, a province is generated at a random location within the mantle until every mantle element has been assigned to a province at least once, or a minimum of one hundred spheres have been created. Because the chemistry of Mercury's crust and mantle is still a matter of debate (Nittler et al. 2011; Weider et al. 2012; Zolotov et al. 2013), we retain full generality by tracking the mixing of a hypothetical element, X , whose distribution is heterogeneous in the mantle and initially has zero concentration in the crust. It is most convenient for the model to track the volume fraction of X , ϕ_X . The provinces are assigned an initial ϕ_X following a Gaussian distribution with mean $\overline{\phi_X} = 0.5$ and standard deviation $\sigma = 0.5$. We investigate $D_{prv} = 10, 100, 200, 250, 750,$ and 1000 km. The thickness of the crust is varied from $\delta_t = 20$ to 80 km, consistent with the estimated range on Mercury (Smith et al. 2012). For each pair of δ_t and D_{prv} studied, one hundred model mercuries with distinct distributions of mantle chemistry are subjected to a randomly selected bombardment.

2.3. Geometric Model

A single, large, mantle-exhuming impact onto an undisturbed surface creates an ejecta blanket enriched in X ,

$$\phi_{X,ejb} = \phi_{X,t} (1 - \phi_m) + \phi_{X,m} (\phi_m), \quad (2)$$

where $\phi_{X,t}$ and $\phi_{X,m}$ are the volume fractions of element X in the crust and mantle respectively, and ϕ_m is the volume fraction of mantle material within the ejecta blanket,

$$\phi_m = 1 - \left(\frac{V_{ex/t}}{V_{exc}} \right), \quad (3)$$

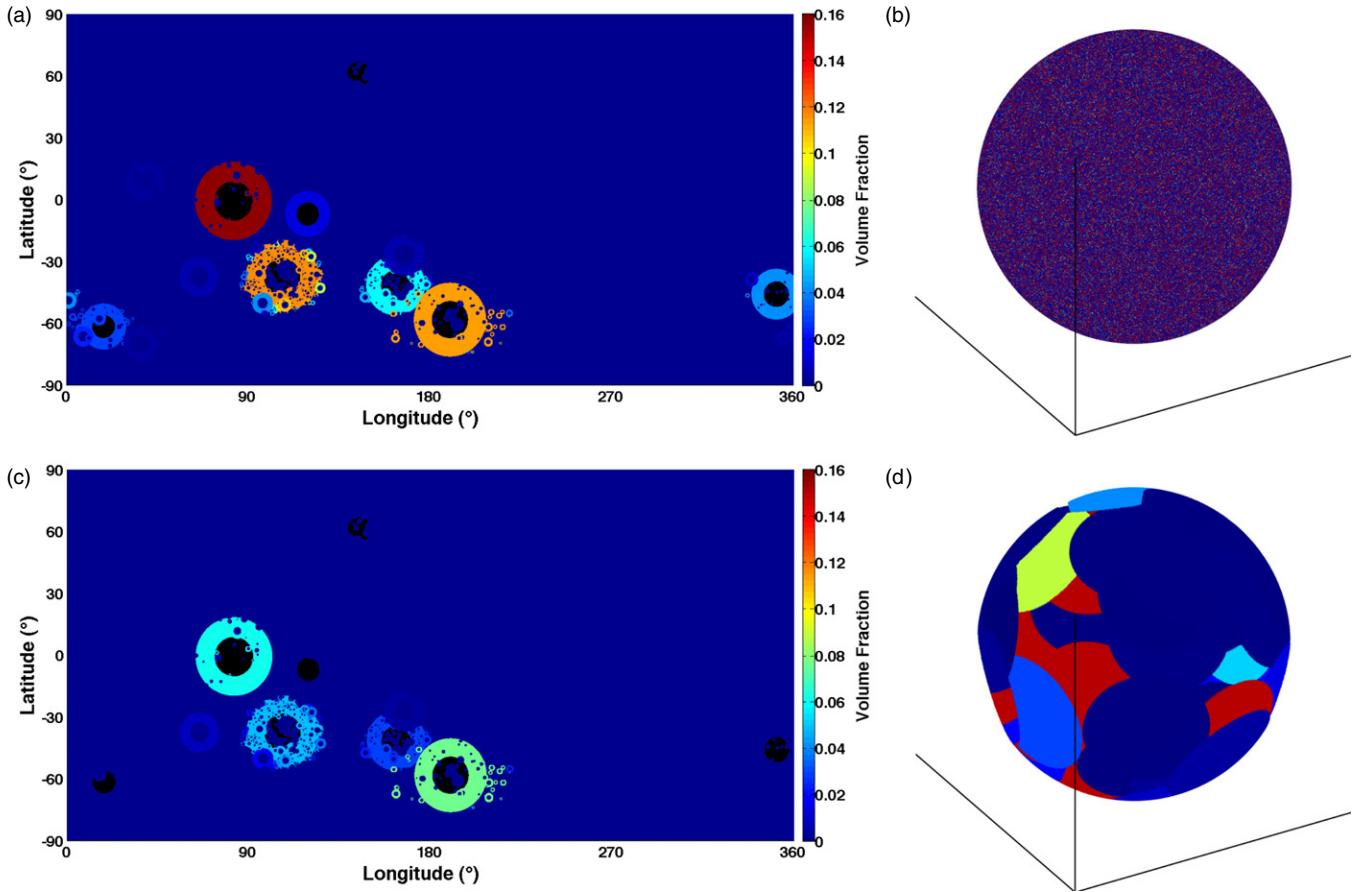


Figure 1. Model results for a single bombardment history onto a mercury with $\delta_t = 50$ km. (a) and (c) Post-bombardment distribution of the volume fraction of element X in ejecta blankets, $\phi_{X,ejb}$, represented by colors, for $D_{prv} = 10$ km, representing a well-mixed mantle untouched by the late veneer (top row) and $D_{prv} = 750$ km, representing a mantle with chemical heterogeneities introduced into Mercury’s mantle during late veneer impacts from large bodies (bottom row). Crater cavities in black denote crust-penetrating impacts. (b) and (d) Global view of mantle provincial heterogeneity, which was modeled as spheres. Colors indicate the volume fraction of element X .

(A color version of this figure is available in the online journal.)

where we define $\phi_m = 0$ for $V_{exc} \leq V_{ex/t}$. The volume of the crust that is excavated during an impact, $V_{ex/t}$, is approximated as a section of a spherical cap,

$$V_{ex/t} = V_{exc} \left[12 \frac{\delta_t}{D_{tc}} - 256 \left(\frac{\delta_t}{D_{tc}} \right)^3 \right]; \quad (4)$$

thus, as δ_t increases, ϕ_m decreases because it is more difficult to excavate mantle.

Repeated and overlapping impacts will cause a deviation from this relationship because $\phi_{X,t}$ will become spatially varying on the surface as impacts onto enriched ejecta blankets redistribute material away from their basin sources and subsequent large impacts eject more mantle material onto the surface. Variations in the distribution of X in the mantle will also cause deviations from this simple model because $\phi_{X,m}$ is not constant in the subsurface. A comparison between the predicted ejecta blanket composition ($\phi_{X,ejb}$) and the simulated values obtained in mantle-exhuming impacts can be used to infer subsurface heterogeneity.

3. RESULTS

Figure 1 shows two model mercuries with $\delta_t = 50$ km hit by identical bombardment histories, but with different distributions of X in the mantle. The top row shows $D_{prv} = 10$ km,

equal to the element size in our model, so that each element has a different ϕ_X ; this represents a well-mixed mantle that is undisturbed by the late veneer, consistent with very small impactors (Schlichting et al. 2012). The bottom row shows a mantle with $D_{prv} = 750$ km, representative of a planet with compositional heterogeneities implanted from large impacts (e.g., Bottke et al. 2010; Raymond et al. 2013). The final ejecta blanket compositions are quite dissimilar. With $D_{prv} = 750$ km, the most mantle-enriched blanket on the surface has $\max(\phi_{X,ejb}) = 0.08$, but for $D_{prv} = 10$ km, $\max(\phi_{X,ejb}) = 0.16$; both these values occur in a crater with $D_{tc} \sim 730$ km. If the mantle was homogenous with $\phi_{X,m} = 0.5$ and the impact occurred onto an undisturbed region, this crater would have $\phi_{X,ejb} = 0.13$ Equation (2). Thus, subsurface heterogeneity affects ejecta blanket composition in a noticeable way.

We perform a suite of Monte Carlo simulations for a range of δ_t and D_{prv} , performing 100 realizations for each pair of parameters. In each simulation, we record $\phi_{X,ejb}$ for each crater and calculate the square of the error between the simulated crater and the value predicted from Equation (2) for each mantle-exhuming impact. For each Monte Carlo run, we find the mean-squared error (MSE). Evidence of subsurface heterogeneity is expressed most intensely in the test statistic,

$$\varepsilon = \frac{\text{MSE}}{\phi_{cal,ejb}}, \quad (5)$$

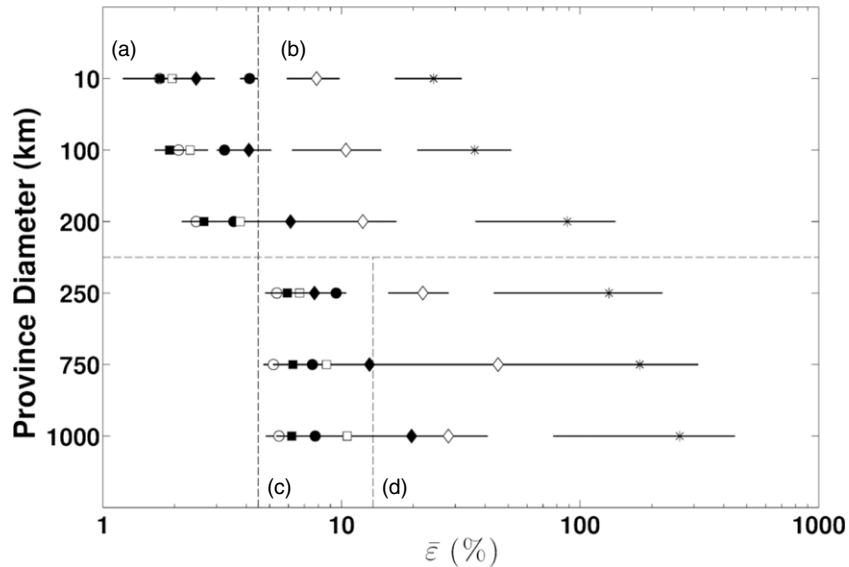


Figure 2. Simulated results for $\bar{\varepsilon}$ with error to a 95% confidence limit (lines). Values are represented by symbols, which also denote crustal thickness: $\delta_t = 20$ km (closed circle), $\delta_t = 30$ km (open circle), $\delta_t = 40$ km (closed square), $\delta_t = 50$ km (open square), $\delta_t = 60$ km (closed diamond), $\delta_t = 70$ km (open diamond), and $\delta_t = 80$ km (asterisk). There are two zones with mostly indistinguishable values denoted as (a) and (c). Zones (b) and (d) are for $\delta_t > 60$ km. Values within these zones are mostly distinct in crustal thickness, but not in province diameter. Additionally $\delta_t = 70$ km in zone (b) is not distinguishable from zone (c) while $\delta_t = 80$ km in zone (b) is not distinguishable from zone (d). The vertical and horizontal dashed lines delineate the zones.

where $\phi_{\text{cal,ejb}}$ is the value of $\phi_{X,\text{ejb}}$ for Mercury’s Caloris basin for each δ_t studied. Caloris is the largest basin on Mercury, so the global maximum of $\phi_{X,\text{ejb}}$ should occur in the Caloris ejecta. Because the value of $\phi_{X,\text{ejb}}$ is sensitive to δ_t , by scaling our results against the ejecta blanket composition of Caloris, we are able to distill the effect of variations in D_{prv} .

Figure 2 shows values of $\bar{\varepsilon}$ averaged over 100 Monte Carlo runs ($\bar{\varepsilon}$) for each pair of δ_t and D_{prv} with corresponding standard error of the means (SEM) to a 95% confidence level. This figure illustrates how the behavior of $\bar{\varepsilon}$, and specifically the magnitude of the SEM, varies as a function of δ_t and D_{prv} . In Figure 3, $\bar{\varepsilon}$ is plotted in 3D space as a function of δ_t and D_{prv} , where colors are interpolated in between studied pairs of δ_t and D_{prv} . We find two shifts in the behavior of $\bar{\varepsilon}$, one at $\delta_t \sim 60$ km and one at $D_{\text{prv}} \sim 250$ km, dividing the parameter space into four different zones of behavior, denoted in Figure 2.

The change in behavior as a function of δ_t arises because the number of crust-penetrating impacts depends strongly on crustal thickness; for $\delta_t \geq 60$ km there are, on average, less than five mantle-exhuming projectiles. Although the values of $\bar{\varepsilon}$ are large for $\delta_t \geq 60$ km, small-number statistics give rise to large error bars on $\bar{\varepsilon}$, and thus, it would be difficult to deduce D_{prv} on mercuries with a thick crust due to limited exposures of mantle material on the surface. When $\delta_t < 60$ km, though, values of $\bar{\varepsilon}$ are smaller and more tightly clustered around a mean. This argues for two δ_t regimes: thin (zones (a) and (c) in Figure 2) and thick (zones (b) and (d) in Figure 2).

The change in behavior for $D_{\text{prv}} \gtrsim 250$ km arises when the characteristic D_{tc} is comparable to D_{prv} . A lower bound on the probability of excavating a province can be estimated from the probability that an impactor lands in the center of a province. If $D_{\text{prv}} \geq D_{\text{tc}}$, the probability of a direct hit on a province is, roughly, the ratio between the cross-sectional area of the province and the planet’s surface area. Once $D_{\text{tc}} > D_{\text{prv}}$, the probability of excavating a given province is equal to the ratio between the surface area of the characteristic crater divided by the surface area of the planet. This produces an abrupt change in behavior at $D_{\text{prv}} \sim 250$ km. Figure 3 shows that the boundary

is slightly curved. This is likely because $\bar{\varepsilon} \propto \phi_{\text{cal,ejb}}^{-2}$. Because $\phi_{X,\text{ejb}}$ decreases with increasing crustal thickness and $\phi_{\text{cal,ejb}}$ is roughly the maximum surface abundance of X , $\phi_{\text{cal,ejb}}$ strongly dominates MSE for $\delta_t \geq 60$ km, causing the observed curvature. This results in two size regimes for D_{prv} : small (zones (a) and (b) in Figure 2) and large (zones (c) and (d) in Figure 2).

The average mercurian crustal thickness is $\delta_t \sim 50$ km (Smith et al. 2012); therefore, Mercury is most likely in the thin crust regime (zones a and c). In this regime, $\bar{\varepsilon}$ is largely insensitive to crustal thickness. With 95% confidence, zone (a) has $1.4\% \leq \bar{\varepsilon} \leq 4.5\%$ with an average of $2.6\% \pm 0.8\%$. Zone (c) has $4.7\% \leq \bar{\varepsilon} \leq 13.5\%$ with an average of $7.1\% \pm 1.7\%$. The values of $\bar{\varepsilon}$ in these zones are statistically different from each other, allowing for determination of the length-scale of mantle heterogeneity from measurements of ejecta blanket composition.

4. CONCLUSIONS

Estimates of the size of late veneer impactors, a key control in the final dynamical states of the terrestrial planets, range from meters to thousands of kilometers in diameter (Bottke et al. 2010; Schlichting et al. 2012; Raymond et al. 2013). Our results suggest the length-scale of chemical heterogeneity in Mercury’s mantle can be constrained from the composition of ejecta blankets in its ancient, heavily cratered terrains. Bombardment by large late veneer objects is a likely means of introducing such heterogeneity. Model mercuries with identical impact histories and different distributions of major elements in their mantles display statistically meaningful differences in the compositions of their ejecta blankets. The length-scale of mantle heterogeneity can be deduced from calculating the mean squared difference between the amount of mantle material mixed into ejecta blankets of mantle-exhuming impacts and the amount predicted by a simple geometric model.

Mercury’s $\delta_t \sim 50$ km (Smith et al. 2012). In this case, $\bar{\varepsilon}$ will be largely insensitive to δ_t , permitting estimates of D_{prv} . If the late veneer was delivered by meter-scale bodies

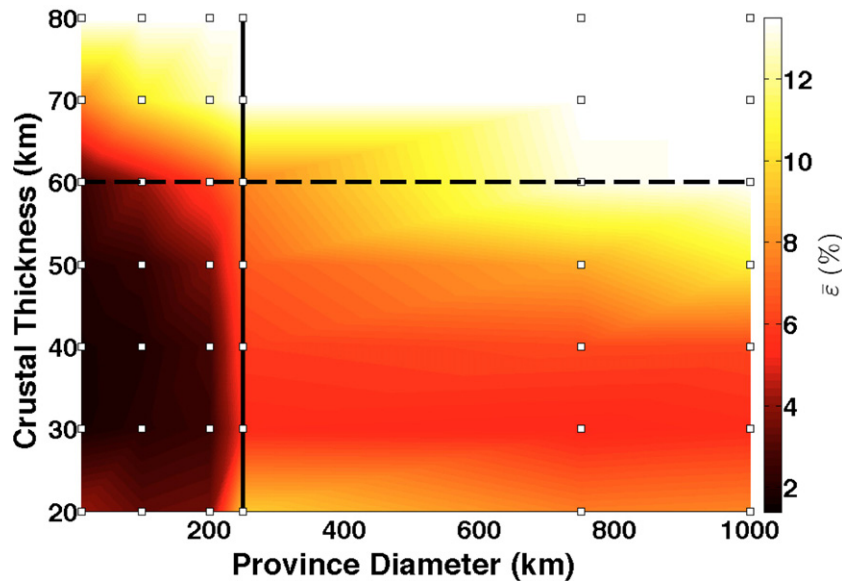


Figure 3. Results for $\bar{\varepsilon}$ in percent (open squares) represented by colors plotted in 3D space against province diameter and crustal thickness. Values in between our simulations are interpolated. The small province regime appears as the dark lobe and is separated from the large province regime by the curved red zone and by the vertical line. Values for $\delta_t > 60$ km (dashed line) are affected by small-number statistics and appear in the mostly white region. Deviations from smooth trends may be due to Monte Carlo methods.

(A color version of this figure is available in the online journal.)

(Schlichting et al. 2012), the mantle would not harbor large compositionally distinct provinces because the late veneer impactors are too small to reach the mantle (e.g., Figures 1(a) and (b)). The relative abundance of mantle-tracer elements in mercurian ejecta blankets would then fall within the small province regime. In this case, we find $\bar{\varepsilon} \lesssim 4\%$, with most values clustering near $\bar{\varepsilon} \approx 3\%$. Values within the small province regime, though, could also imply that Mercury has undergone vigorous convection and its mantle is homogeneous. If the late veneer was delivered by bodies with diameters >250 km (Bottke et al. 2010; Raymond et al. 2013), ejecta blanket compositions will deviate significantly from a simple geometric model (e.g., Figures 1(c) and (d)). In this case, we find $\bar{\varepsilon} \gtrsim 5\%$, with most values near $\bar{\varepsilon} \approx 7\%$. Additionally, if observations suggest large provinces, this would also imply that Mercury has avoided vigorous convection during its history.

We have intentionally made no assumption about the compositions of the mantle and crust of Mercury, other than to suppose there exists an element X that is abundant in the mantle and has essentially zero concentration in the crust. The Mercury Surface, Space ENvironment, Geochemistry, and Ranging (MESSENGER) gamma-ray and X-ray spectrometer have been used to map the mercurian surface chemistry and, by correlating with landforms, infer subsurface compositions (Nittler et al. 2011; Evans et al. 2012; Peplowski et al. 2012; Weider et al. 2012). Once a suitable mantle-tracer element is deduced from MESSENGER data, and its concentration measured in ejecta, the subsurface abundance and distribution of the tracer element can be estimated by measuring its volume fraction within the ejecta blankets of mantle-exhuming impacts. Estimating the average ε for all crust-penetrating craters globally would yield a constraint on D_{prv} and late veneer impactor size.

We thank an anonymous reviewer for valuable comments that helped to improve this manuscript. This work was supported by

NASA through the Center for Lunar Origin and Evolution under the NASA Lunar Science Institute grant NNA09DB32A and the Planetary Geology and Geophysics program through grant PG&G NNX12AI76G.

REFERENCES

- Barr, A. C., & Canup, R. M. 2010, *NatGe*, 3, 164
Benz, W., Anic, A., Horner, J., & Whitby, J. A. 2007, *SSRv*, 132, 189
Bottke, W. F., Durda, D. D., Nesvorný, D., et al. 2005, *Icar*, 175, 111
Bottke, W. F., Vokrouhlický, D., Minton, D., et al. 2012, *Natur*, 485, 78
Bottke, W. F., Walker, R. J., Day, J. M. D., et al. 2010, *Sci*, 330, 1527
Britt, D. T., Yeomans, D., Housen, K., et al. 2002, in *Asteroids III*, ed. W. Bottke et al. (Tucson, AZ: Univ. Arizona Press), 485
Chambers, J. E. 2004, *E&PSL*, 223, 241
Chambers, J. E., & Wetherill, G. W. 1998, *Icar*, 136, 304
Day, J. M. D., Pearson, D. G., & Taylor, L. A. 2007, *Sci*, 315, 217
Day, J. M. D., Walker, R. J., James, O. B., et al. 2010, *E&PSL*, 289, 595
Drake, M. J., & Righter, K. 2002, *Natur*, 416, 39
Evans, L. G., Starr, R. D., Weider, S. Z., et al. 2012, *JGRE*, 117, E00L07
Gomes, R., Levison, H. F., Tsiganis, K., et al. 2005, *Natur*, 435, 466
Hartmann, W. K., Ryder, G., Dones, L., et al. 2000, in *Origin of the Earth and Moon*, ed. R. M. Canup et al. (Tucson, AZ: Univ. Arizona Press), 493
Hauck, S. A., Margot, J.-L., Solomon, S. C., et al. 2013, *JGRE*, 118, 1
Housen, K. R., & Holsapple, K. A. 2011, *Icar*, 211, 856
Ivanov, B. A., & Artemieva, N. A. 2002, *GSASP*, 356, 619
Ivanov, B. A., Neukum, G., Bottke, W. F., et al. 2002, in *Asteroids III*, ed. W. F. Bottke et al. (Tucson, AZ: Univ. Arizona Press), 89
Kleine, T., Touboul, M., Bourdon, B., et al. 2009, *GeCoA*, 73, 5150
Le Feuvre, M., & Wieczorek, M. A. 2011, *Icar*, 214, 1
Lewis, J. S. 1972, *Sci*, 186, 440
Maxwell, D. E. 1977, in *Impact and Explosion Cratering*, ed. D. J. Roddy et al. (New York: Pergamon), 1003
Melosh, H. J. 1989, in *Impact Cratering: A Geologic Process* (New York: Oxford Univ. Press)
Michel, N. C., Hauck, S. A., Solomon, S. C., et al. 2013, *JGRE*, 118, 1033
Morbidelli, A., Marchi, S., Bottke, W. F., et al. 2012, *E&PSL*, 355, 144
Nittler, L. R., Starr, R. D., Weider, S. Z., et al. 2011, *Sci*, 333, 1847
O'Neil, H. S. C. 1991, *GeCoA*, 55, 1159
Osinski, G. R., Tornabene, L. L., & Grieve, R. A. F. 2011, *E&PSL*, 210, 167
Peplowski, P. N., Lawrence, D. J., Rhodes, E. A., et al. 2012, *JGRE*, 117, E00L04

Raymond, S. N., Schlichting, H. E., Hersant, F., & Selis, F. 2013, *Icar*, **226**, 671
Redmond, H. L., & King, S. D. 2007, *PEPI*, **164**, 221
Schlichting, H. E., Warren, P. H., & Yin, Q.-Z. 2012, *ApJL*, **752**, 8
Smith, D. E., Zuber, M. T., Phillips, R. J., et al. 2012, *Sci*, **336**, 214
Tera, F., Papanastassiou, D. A., & Wasserburg, G. J. 1974, *E&PSL*, **22**, 1

Tsiganis, K., Gomes, R., Morbidelli, A., et al. 2005, *Natur*, **435**, 459
Walker, R. J. 2009, *ChEG*, **69**, 101
Walker, R. J., Horan, M. F., Shearer, C. K., et al. 2004, *E&PSL*, **224**, 399
Weider, S. Z., Nittler, L. R., Starr, R. D., et al. 2012, *JGRE*, **117**, E00L05
Wood, B. J., Walter, M. J., & Wade, J. 2006, *Natur*, **441**, 825
Zolotov, M. Y., Sprague, A. L., Hauck, S. A., et al. 2013, *JGRE*, **118**, 138